This article has been accepted for publication in a future issue of this journal, but has not been fully edited. Content may change prior to final publication. Citation information: DOI 10.1109/LRA.2018.2801469, IEEE Robotics and Automation Letters

Bundled Super-Coiled Polymer Artificial Muscles: Design, Characterization, and Modeling

Anthony Simeonov, Taylor Henderson, Zixuan Lan, Guhan Sundar, Adam Factor, Jun Zhang and Michael Yip

***Abstract*—Super-coiled polymer (SCP) artificial muscles have many attractive properties such as high energy density, large contractions, and good dynamic range. To fully utilize them for robotic applications, it is necessary to determine how to scale them up effectively. Bundling of SCP actuators, as though they are individual threads in woven textiles, can demonstrate the versatility of SCP actuators and artificial muscles in general. However, this versatility comes with a need to understand how different bundling techniques can be achieved with these actuators and how they may trade off in performance. This paper presents the first quantitative comparison, analysis, and modeling of bundled SCP actuators. By exploiting weaving and braiding techniques, three new types of bundled SCP actuators are created: woven bundles, two-dimensional (2D) and three-dimensional (3D) braided bundles. The bundle performance is adjustable by employing different numbers of individual actuators. Experiments are conducted to characterize and compare the force, strain, and speed of different bundles, and a linear model is proposed to predict their performance. This work lays the foundation for model-based SCP-actuated textiles, and physically scaling robots that employ SCP actuators as the driving mechanism.**

***Index Terms*—Hydraulic/Pneumatic Actuators, Biomimetics, Artificial Muscle Actuators**

I. Introduction

TRADITIONAL robot actuation predominantly utilizes electric motors with reduction gears and rigid transmissions, which are often heavy, costly, and unsafe. With the shift toward compliant, soft, and flexible robots that operate effectively with humans and biomimetic structures, artificial muscle actuators have attracted a great deal of attention [1]. Their muscle-like properties, like high power-to-weight ratio and inherent compliance, open doors toward novel robotic applications such as biomimetic robots, soft robots, robotic prosthetics and exoskeletons, medical robots, and many others [2]–[6]. The recently developed super-coiled polymer (SCP) actuators have displayed strong potential as the next state-of-the-art artificial muscle technology. They have demonstrated significant power-to-weight ratio up to 5.3 kW/kg, large strain over 20%, and good dynamic range over 1 Hz in a thin, lightweight, and muscle-like form factor [7]–[9].

SCP actuators can contract and expand when heated and cooled. Since their creation [7], a rapid increase of research efforts have been devoted to understand and utilize them for robotic applications. Different materials have been tested to manufacture SCP actuators, including carbon nanotube yarns, and more cost-effective nylon fishing lines and sewing threads [7], [8], [10]. By coating the threads with conductive materials, electric current can be used to control SCP actuators via Joule heating [11]. Their thermoelectrical and thermomechanical properties have been measured under different environmental conditions [9]. To characterize and estimate the performance of SCP actuators, both physics-based and data-driven models have been presented [8], [9], [12], [13]. With the evident advantages of SCP actuators, they have been actively explored as driving mechanisms for a wide variety of robotic applications, such as robotic fingers, hands, and arms [9], [14], [15], soft robots [16], assistive robots [17], and wearable applications [18].

To fully unleash the potential of SCP actuators as robot muscles, further studies are needed to determine how to scale them up to be more powerful. An individual SCP actuator can only produce about 1 N of force, which is often insufficient for robotic systems [11], [17]. Enabling a larger force through bundling multiple SCP actuators has shown to be a highly effective solution. By using multiple SCP actuators in parallel, the bundled actuator could produce a larger force [9], [15]. For example, 16 N of force was achieved by bundling 16 SCP actuators [19]. A bundled SCP actuator was manufactured by weaving [18]. Several textile configurations were developed by braiding a large number of SCP actuators [8]. With the successful demonstrations of bundling approaches above, it would be extremely useful to follow with a quantitative comparison and modeling to gain further insight into designing bundles for SCP actuators. This would significantly improve the versatility of these actuators and has not yet been investigated.

Several different methods have been developed for amplifying force in other types of artificial muscles. A stronger actuator could be created with a larger cross-sectional area for increased force output, however, other important properties of the actuator could be compromised. For example, the speeds of thicker shape memory alloy (SMA) actuators were much slower [20], and the compliance and compactness of thicker McKibben actuators were reduced [21]. Similar to SMA actuators, by thickening SCP actuators, the speeds would be largely compromised due to the increased heat penetration depth. Producing a thicker SCP actuator is thus an undesirable

Manuscript received: September, 10, 2017; Revised December, 16, 2017; Accepted January, 14, 2018.

This paper was recommended for publication by Editor Paolo Rocco upon evaluation of the Associate Editor and Reviewers' comments.

Anthony Simeonov and Zixuan Lan are with the Department of Mechanical and Aerospace Engineering, University of California, San Diego, La Jolla, CA 92093, USA (e-mail: asimeono@ucsd.edu; zilan@ucsd.edu)

Taylor Henderson, Guhan Sundar and Adam Factor are with the Department of Bioengineering, University of California, San Diego, La Jolla, CA 92093, USA (e-mail: tjwest@ucsd.edu; gusundar@ucsd.edu; ajfactor@ucsd.edu)

Jun Zhang and Michael Yip are with the Department of Electrical and Computer Engineering, University of California, San Diego, La Jolla, CA 92093, USA (e-mail: j5zhang@ucsd.edu; yip@ucsd.edu)

Digital Object Identifier (DOI): see top of this page.

This article has been accepted for publication in a future issue of this journal, but has not been fully edited. Content may change prior to final publication. Citation information: DOI 10.1109/LRA.2018.2801469, IEEE Robotics and Automation Letters

approach.

Additionally, bundling multiple actuators in parallel also allows for force amplification. For example, by mechanically combining 48 SMA actuators in parallel, the overall actuator could lift up to 45.4 kg of weight without compromising the speeds [22]. It was shown that bundling thin McKibben actuators in parallel allowed for increased force [21], [23]. It was further demonstrated that through variable recruitment control of bundled pneumatic and fluidic actuators, the efficiency could be improved [24], [25]. Unfortunately, incorporating multiple individual actuators with parallel placement configurations leads to a lack of unified structure, increased size, low robustness, increased modeling difficulty considering the contributions of each actuator, and an overall complicated system with integration challenges.

Finally, bundling through active knits, weaves, and braids can be employed to effectively increase the force output. For example, an SMA knitted textile was developed to produce a significant amount of force [26]. A knitting procedure was proposed using Spandex and carbon nanotube yarns [27], enabling a maximum power output of 1.28 kW/kg. More recently, different configurations of knitted and woven polymer artificial muscles were further developed [28]. These bundles each maintain the muscle-like properties of the individual strands while achieving the desired strength increase. Further, weaves and braids provide many advantages over parallel bundling, including a unified and stable structure, compact size, and a readiness for integration. While the complexity of fabricating the bundled actuator does increase due to the bundling process, the system level complexity is reduced.

This paper presents the *first* study to quantitatively compare, analyze, and model bundled SCP actuators. Exploiting different weaving and braiding techniques, three new types of SCP bundled actuators are manufactured: woven bundles, two-dimensional (2D) and three-dimensional (3D) braided bundles. A set of woven and braided bundles are fabricated with different numbers of individual actuators. The performance of different bundles are compared in terms of force production, strain, and speed. It is verified that the proposed bundles produce linearly amplified force with an increased number of employed actuators. To estimate the performance, a model incorporating the bundle configuration is presented. The analysis suggests that 2D braided bundles actuate faster and consume less power, woven bundles are stiffer, and the 3D braided bundle displays especially large stiffness and force range at the cost of slower speed and more complex fabrication.

The overall combination of models and characterization trends in this work will close the design utility gap between SCP actuators and traditional actuators. For example, the models of motors between voltage and speed with different volumes and weights are readily available, which enables their wide adoption for diverse applications. Similarly, the comparison and models of bundled SCP actuators are fundamental in enabling engineers and roboticists to strategically choose actuators which meet design specifications, instead of playing guess-and-check until something works. By identifying these models and trends for a set of bundle configurations, this study marks the first step toward enabling engineers to navigate a deliberate design process with SCP actuators for a variety of applications.

(a) (b) (c)

Fig. 1. Samples of three different bundled SCP actuators. (a) A woven bundle made of 6 actuators. (b) A 2D braided bundle made of 5 actuators. (c) A 3D braided bundle made of 8 actuators.

II. Design and Fabrication

A. Proposed Design

Three types of new bundles were proposed, namely, woven bundles, 2D and 3D braided bundles, with a few samples shown in Fig. 1. All of the bundles were made by hand. We focused on bundles which met the criteria of providing amplified force with equivalent strain, being easy to fabricate by hand, and which are scalable in size. The braids and weaves under study in this work represent a range of bundles which meet these criteria. It is noted that other types of woven bundles and braided bundles have been presented [10]. Other configurations such as stitched and knitted bundles could also be realized. However, considering the complicated fabrication procedure for the stitched bundle [26] and lacking force amplification performance of the knitted bundle [28], those approaches were not studied in this work.

The woven bundles were analogous to simple parallel placement, but with the individual fibers interconnected. Each actuator was directed straight along its axis, and the overall structure was similar to a flat strip of fabric. Braided bundles had individual actuators braided among each other, with no external material to provide the connected structure. Each fiber underwent directional changes through braiding and the form was more rope-like. 2D braids and a hollow 3D braid were developed to highlight the range of available braiding options.

B. Fabrication Procedure

The fabrication procedures of the proposed bundles are summarized. The fabrication of individual SCP actuators is provided in Section IV.A.

1) Woven Bundle: To create the woven bundle, each actuator was aligned in parallel and a weave was threaded over and under each actuator to form a unified structure [28], as illustrated in Fig. 2(a). To permit adequate spacing for cooling and maintain uniformity, each weave was made to have a weave density of about 2 turns/cm and at least 1 mm spacing between actuators. Cotton string was utilized as an easily configurable and low-cost weave. Other types of weaves could also be adopted.

This article has been accepted for publication in a future issue of this journal, but has not been fully edited. Content may change prior to final publication. Citation information: DOI 10.1109/LRA.2018.2801469, IEEE Robotics and Automation Letters

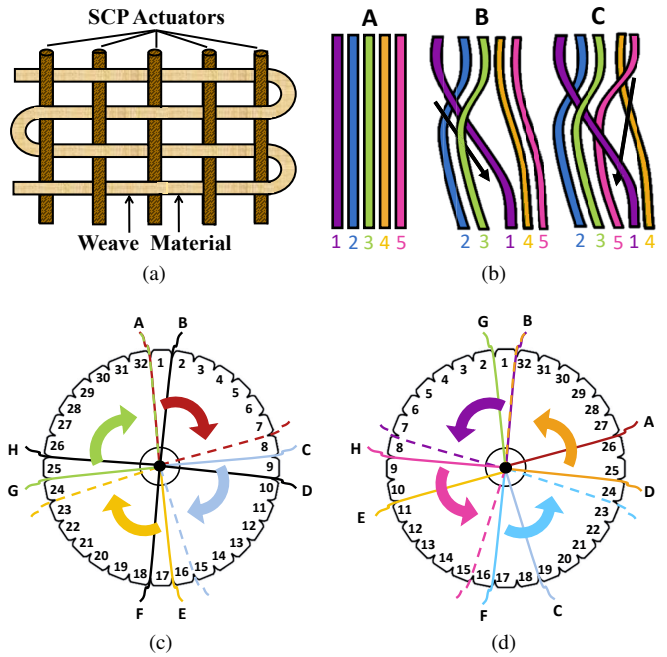

Fig. 2. The schematics of the (a) woven bundle, (b) odd-numbered 2D braided bundle, and 3D braided bundle at (c) step 1 (clockwise motion) and (d) step 2 (counter-clockwise motion).

2) 2D Braided Bundle: The braiding method depended on whether the adopted number of actuators was odd or even. Both started with assigning numbers to each strand, as shown for a braid of 5 actuators in Fig. 2(b). Fabricating odd-numbered braids involved the repetition of moving the leftmost strand to the middle, followed by the rightmost strand to the middle. Similarly, even-numbered braids involved moving the rightmost strand to the right-middle and the second-leftmost strand all the way to the right. The mirrors of these steps were then performed starting with the new leftmost strand. The whole process was repeated for the entire braid length. For all 2D braided bundles, the movement of a strand occurred by threading over and under the strands in between, as shown in Fig. 2(b) for a braid of 5 actuators.

3) 3D Braided Bundle: Fabrication of the 3D braided bundle followed the Kumihimo form of braiding [29]. As seen in Fig. 2(c)-(d), 4 pairs of actuators (A–B, C–D, E–F, G–H) were placed evenly around the circumference of a circular Kumihimo disc. Each actuator was held in one of the outer notches and held in constant tension by a weight in the central disc opening. In the first step, the leftmost strand of each pair (A, C, E, G) was sequentially brought clockwise over its neighbor and placed in the notch closest to the next actuator, as shown in Fig. 2(c). This formed 4 new pairs (G–B, A–D, C–F, E–H). In the second step, the rightmost strand of each pair (B, D, F, H) is then brought counter-clockwise over its new neighbor and placed in the notch closest to the next actuator, as illustrated in Fig. 2(d). The two steps were repeated for the entire length of the braid.

4) Fabrication Results: Woven bundles made of 3–7 actuators, 2D braided bundles made of 3–6 actuators, and a 3D braided bundle made of 8 actuators were fabricated. Table I lists the fabrication details for each bundle and the overall group of individual SCP actuators, where n is the number of individual actuators within each bundle, "Turn" denotes the total number of weave turns within the weave bundle, and "Repeat" is the number of times one of the actuators within the braid ends up back in its original position [29]. As seen, good consistencies were achieved during the fabrication.

TABLE I
BUNDLED SCP ACTUATOR FABRICATION PARAMETERS

		Individual SCPs		
	Length (mm)	Resistance (Ω)		
	220 ± 20	18.0 ± 2.5		
		Weave		
n	Length (mm)	Resistance (Ω)	Turn	Spacing (mm)
3	209 ± 1	6.75 ± 0.05	42	1.02 ± 0.4
4	213 ± 3	5.1 ± 0.1	43	1.36 ± 0.02
5	191 ± 2	3.35 ± 0.15	41	1.47 ± 0.05
6	198 ± 6	2.8 ± 0.1	42	1.21 ± 0.09
7	196 ± 4	2.2 ± 0.2	39	1.24 ± 0.06
		2D Braid		
n	Length (mm)	Resistance (Ω)	Repeat	
3	199 ± 1	5.4 ± 0.1	5	
4	185 ± 1	4.45 ± 0.15	5	
5	189 ± 1	4.15 ± 0.05	5	
6	201 ± 1	3.25 ± 0.05	7	
		3D Braid		
n	Length (mm)	Resistance (Ω)		
8	175 ± 1	2.75 ± 0.05		

III. MODELING

In this section, a linear model is proposed for the bundled actuators. The model is derived based on the linear model for individual SCP actuators [9], [17]. It is noted that even though physical models will be helpful [12], this study adopted experimental models as a preliminary quantitative analysis of bundled SCP actuators. Although the model does not reflect behavior up to the limits of applied stress and input power, it has shown to be effective in describing the behavior of SCP actuators under practical operating conditions.

A. A Single SCP Actuator

The thermal dynamics of an SCP actuator operated through Joule heating have been shown to behave similarly as a first order linear system [9] described by

$$C_{\text{th}} \frac{dT}{dt} = P(t) - \lambda (T - T_0), \tag{1}$$

where C_{th} and λ are the thermal mass and absolute thermal conductivity of the actuator, respectively, T is the temperature of the actuator, T_0 is the ambient temperature, and $P(t)$ is the input electrical power at time t. To quantify the speed of the dynamics, the time constant, $\tau = \frac{C_{\text{th}}}{\lambda}$, can be adopted. Under steady-state condition, a constant temperature is reached, and $P(t) = \lambda (T - T_0)$.

The thermo-mechanical properties of SCP actuators can be described as a spring-damper system with an added temperature dependent term, which is expressed as [9]

$$F = k(x - x_0) + b\dot{x} + c(T - T_0), \tag{2}$$

This article has been accepted for publication in a future issue of this journal, but has not been fully edited. Content may change prior to final publication. Citation information: DOI 10.1109/LRA.2018.2801469, IEEE Robotics and Automation Letters

where x and x_0 are the loaded length and resting length of the actuator, respectively, k represents the stiffness, b is a damping term, and c denotes the force per change in temperature. Under steady-state conditions, $\dot{x} = 0$.

The overall model can be obtained by combining Eq. (1) and Eq. (2) together. Under steady-state condition, the overall model describes the quasi-static relationship among steady-state force, length, and actuator power input:

$$F = k(x - x_0) + \frac{c}{\lambda} P. \tag{3}$$

The effect of different convective environments on thermal constants in the model has been studied in depth for individual SCP actuators [9]. In this work, we consider a standing air environment with constant temperature and air flow condition.

B. Normalization Metrics

To facilitate the comparison of different bundled SCP actuators with varying lengths and sizes, normalized metrics including the unit strain and unit power are introduced.

1) Unit Strain: The metric of unit strain is useful for comparing contractions of bundles with different lengths. The unit strain, Δx_u, is defined as

$$\Delta x_u = \frac{x - x_0}{x_0}. \tag{4}$$

The loaded length of the bundled actuator, x, can be measured by additional position sensors. The resting length, x_0, can be determined in this way: with the bundled actuator laying fully extended on a counter, measure the average of the active portion of each actuator in a bundle. Due to the good fabrication consistency for single SCP actuators (shown in Table I), the length of the bundle is very close to the length of each individual actuators.

2) Unit Power: Electric power is a more appropriate input than voltage, because the temperature of the actuator is dependent on power [8], [9], as shown in Eq. (1). The adoption of unit power is important – due to the parallel combination of multiple actuators, measuring against power directly does not provide intuitive comparison. The total power drawn also depends on the bundle size and length. Therefore, by normalization, we can easily compare the force production versus unit power for bundles of different configurations. The unit power, P_u, is expressed as

$$P_u = \frac{P}{n \cdot x_0}, \tag{5}$$

where P is the overall electrical power input, and n is the number of individual actuators of the bundle.

C. Bundled SCP Actuators

The bundled SCP actuator can be considered as a unified actuator exhibiting similar properties of single SCP actuators. Existing models for SCP actuators can thus be adapted [9]. The difference is that the bundle configuration, denoted as g, is an additional parameter of the model. The thermal dynamics can be approximated as

$$C_{\text{th}}(g)\frac{dT}{dt} = P(t) - \lambda(g) \cdot (T - T_0). \tag{6}$$

Under steady-state conditions, the thermo-mechanical-electrical model can be simplified to

$$F = k(g)(x - x_0) + \frac{c(g)}{\lambda(g)} P. \tag{7}$$

Converting to the metrics of unit strain and unit power as defined in Eq. (4) and Eq. (5), the final model describing the steady-state relationship is

$$F = K(g)\Delta x_u + q(g) P_u, \tag{8}$$

where the parameter K denotes stiffness and q represents thermal properties. Clearly, large K and q translate to large force produced by the bundled actuator. Note although many bundle configuration parameters may affect the performance, in this study, we strive to fabricate bundles of the same configuration with consistent parameters such as spacing, tightness, and density (Table I). Thus, we consider that the configuration variables at play reduce to the type of bundle and the number of actuators within the bundle, n. The consideration of other configuration variables as model parameters is a future direction of this work.

IV. Experiments and Setup

A. Fabrication of SCP Actuators

SCP actuators were fabricated by a coiling and annealing process. A conductive nylon sewing thread (Technical Textiles, 110/34 dtex HC z-turns) was twisted until it was fully coiled. This coiled thread was double-backed and then thermally annealed by applying voltage pulses. During the annealing, a 200 g weight was hung on the end of the thread. The weight was experimentally determined [9]. After annealing, an SCP actuator was created, which could contract and expand as it was heated and cooled.

The mechanism of contractions can be explained as following: With an increased temperature, the untwisted nylon expands in its radial direction and contracts along its axial direction. By inserting twists to the point of coiling, the thermal expansion character is amplified and very large contractions are achieved upon heating. More details on the fabrication and mechanism can be found in [8], [9], [13].

B. Experimental Setup

Isometric force production and isotonic contraction experiments were conducted to compare the performance of different bundled actuators. In isometric tests, each bundle was held at a fixed length with one end attached to a load cell (ANYLOAD 108BA-3kg) for tension measurements, as shown in Fig. 3(a). Similarly, to conduct isotonic contractions experiments, weights were hung to keep the bundle in constant tension while it was allowed to contract and expand, as illustrated in Fig. 3(b). A linear magnetoresistive sensor (Honeywell SPS-L035-LATS) was used to measure the contraction of the bundled actuator. Data acquisition and input power control were realized using a data acquisition card (NI-USB 6001), National Instruments LabVIEW software, and an amplifier circuit utilizing a power Op-Amp (TI OPA541). Input voltage and sensor signals were collected with the data acquisition

This article has been accepted for publication in a future issue of this journal, but has not been fully edited. Content may change prior to final publication. Citation information: DOI 10.1109/LRA.2018.2801469, IEEE Robotics and Automation Letters

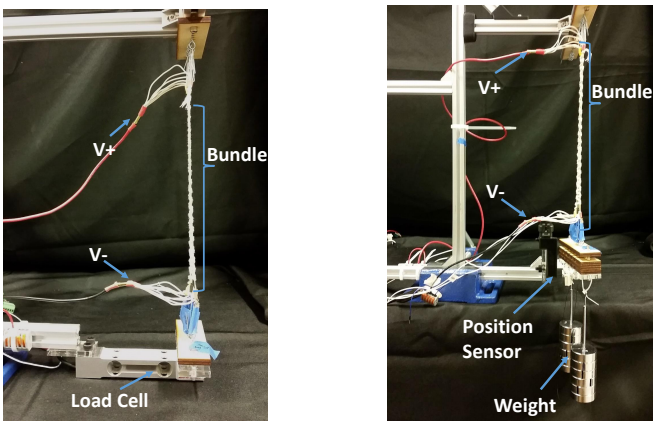

(a) (b)

Fig. 3. (a) Isometric experiment setup for force and power measurements. (b) Isotonic experiment setup for strain and power measurements.

system at 250 Hz throughout this study. More details of the setup can be found in [13], [30].

V. Model Identification

A. Performance Metric

The modeling performance was quantified by the average absolute error and standard deviation percentages:

$$E_{\text{average}} = \frac{\sum_{i=1}^{M} |e_i|/M}{R} \times 100\%, \tag{9}$$

$$\sigma = \frac{\sqrt{\sum_{i=1}^{M} (e_i - \bar{e})^2}}{R} \times 100\%, \tag{10}$$

where M was the number of data-points to be evaluated, e_i denoted the error of the i_{th} point, R was the output range, and $\bar{e}$ was the average error.

B. General Procedure

At the start of each experiment, resistance was measured as a static value. Due to the slight variation in bundle length with different loads, the static resistance slightly changed between tests. This was accounted for by modulating the sequence of input voltages to keep the power operating range for each bundle consistent. The operating range was empirically determined by finding the input voltage required for the bundle to approximately reach a 10% steady-state contraction, which was close to the maximum contraction of the SCP actuators in this study [9], [13].

Each experiment was performed using an input power sequence of 8 incremental increasing and decreasing steps throughout the operating range, as shown in Fig. 4 (top). A similar input sequence has been adopted to capture the major curve of the hysteresis in SCP actuators [13], which is caused by the friction among different coils of the actuator [8], [9], [11]. To observe the full step response, each step was held for 90 seconds for the woven bundles and 2D braided bundles, and 150 seconds for the 3D braided bundle. It is noted that this experiment was conducted to obtain both the transient and quasi-static performance, with similar procedures successfully conducted in [13], [16]. To obtain the steady-state tension and strain, the last 30% of the step responses were averaged to cope with minor disturbances and noise. In this paper, the term "index" refers to the numbering of the steady-state power, strain, and force values.

As an example, under the power sequence in Fig. 4 (top), the transient force and strain were provided for the 3D braided bundle, as shown in Fig. 4 (middle) and Fig. 4 (bottom), respectively. It was noted that the strain transient curves under different loadings exhibited noticeable inconsistencies. This might be caused by the actuator resistance variation during contraction, which has been shown [31]. Accounting for varying resistance was beyond the scope of this work.

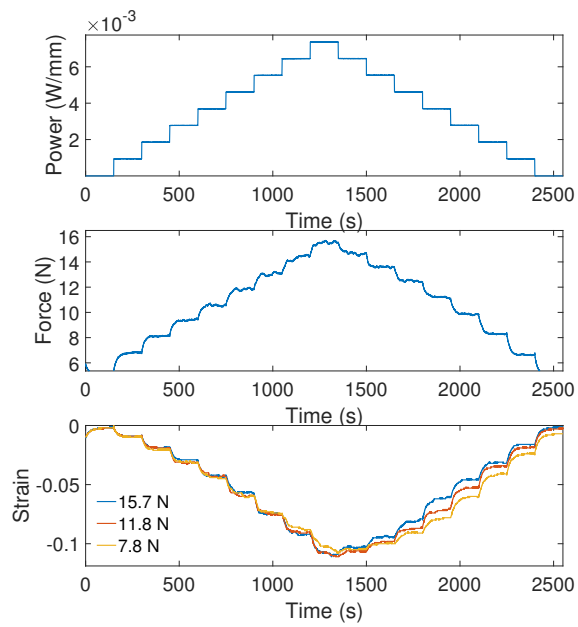

Fig. 4. Experimental measurements of the 3D braided bundle: Unit power input versus time (top), force versus time (middle), and strain versus time at three different loads (bottom).

C. Force Versus Power

To conduct the isometric experiments, a small pretension of 0.3–0.4 N per actuator was utilized to prevent the bundle from being slack [30]. Fig. 5(a) and Fig. 5(b) show the steady-state force versus unit power for each woven and braided bundle, respectively.

To capture the steady-state relationship between the force and power input, the coefficient q in Eq. (8) was identified by fitting the experimental measurements with a linear least-squares regression using MATLAB function *polyfit*. The overall modeling errors for the braided bundles and woven bundles were $1.21 \pm 0.91\%$ and $1.18 \pm 0.81\%$, respectively. The very small errors reflected the approximately linear relationship between force and power in bundled SCP actuators.

D. Strain Versus Power

Isotonic contraction experiments were performed to characterize the scenario where the bundled actuator was used

This article has been accepted for publication in a future issue of this journal, but has not been fully edited. Content may change prior to final publication. Citation information: DOI 10.1109/LRA.2018.2801469, IEEE Robotics and Automation Letters

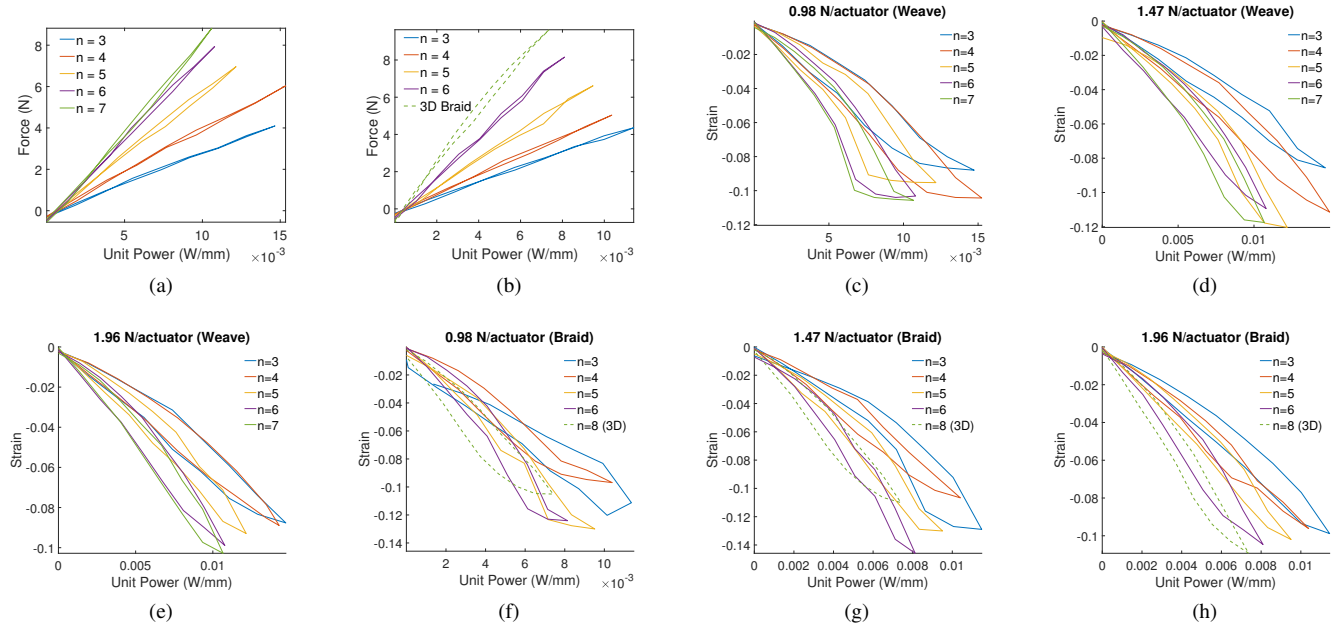

Fig. 5. Steady-state force versus unit power for (a) woven bundles and (b) braided bundles. Steady-state unit strain versus unit power for woven bundles with (c) 0.98 N/actuator, (d) 1.47 N/actuator, and (e) 1.96 N/actuator loads, and for braided bundles with (f) 0.98 N/actuator, (g) 1.47 N/actuator, and (h) 1.96 N/actuator loads.

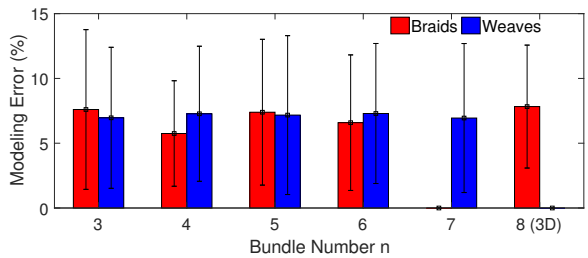

Fig. 6. Modeling error of the steady-state relationship between strain and power for each SCP bundled actuator.

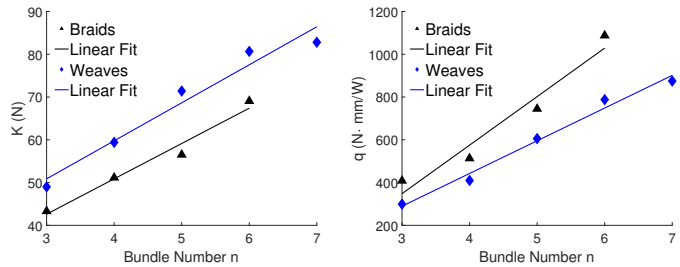

Fig. 7. Model fitting for K versus n (left) and q versus n (right).

to move the position of some mass. Tensions of 0.98 N, 1.47 N, and 1.96 N per actuator were applied with the hanging weights. Fig. 5(c)-(h) shows the measured steady-state relationship between strain and unit power for the bundled actuators under different loads. By measuring full contraction and extension cycles for each bundle, the major strain vs. power hysteresis was captured. The nonlinear loops in Fig. 5(c)-(h) highlight this behavior. Our prior work focused on modeling this hysteresis in individual SCP actuators [13].

Using a similar approach, K was found for each bundle. Fig. 6 shows the average modeling error for each bundle. The error appeared to stay approximately constant regardless of bundle configurations at about 8% or below. The overall modeling errors were $7.72 \pm 7.02\%$ and $7.58 \pm 6.13\%$ for the braided bundles and woven bundles, respectively. These larger errors were expected based off the more prominent hysteresis behavior, which was also found in [9], [11]. The errors were comparable to the existing linear modeling approaches for individual SCP actuators [13], confirming the effectiveness of the proposed model.

E. Overall Model

With the identified parameters of K and q for each bundled actuator, the overall quasi-static model was obtained for each type of bundle. The model identification was realized by fitting the linear relationship between the model parameters and the number of actuators within the bundle. Fig. 7 shows the K and q, as well as the linear fittings. The identified models for each bundle type were

$$K_{\text{braid}} = 8.26n + 17.83, \tag{11}$$

$$K_{\text{weave}} = 8.89n + 24.21, \tag{12}$$

$$q_{\text{braid}} = 226.88n - 332.55, \tag{13}$$

$$q_{\text{weave}} = 152.93n - 169.26, \tag{14}$$

and the K and q values for the 3D braided bundle were 95.22 N and 1418.5 N·mm/W, respectively. It was shown that the model could accurately capture the performance of bundled actuators with different configurations with a relatively small error: the average error percentages of K and q were 6.9% and 4.1% for the woven bundles, and 5.1% and 8.8% for the 2D braided bundles. The trends showed that weaves were generally stiffer than braids and braids produced more force

This article has been accepted for publication in a future issue of this journal, but has not been fully edited. Content may change prior to final publication. Citation information: DOI 10.1109/LRA.2018.2801469, IEEE Robotics and Automation Letters

and larger contractions than weaves, as shown in Fig. 7 (left). The larger stiffness of the weaves was likely because the presence of the cotton reduced the ability of linear motions for the weave. Fig. 7 (right) shows that q for braids scaled more rapidly than for weaves, which was likely related to the fact that the conductive heat was shared between the nylon in the braid, versus the analogous conduction with the cotton in the weaves.

F. Dynamics

Similarly as in [9], force could be used as an indirect measurement of temperature. To quantify the speed of the actuators' thermoelectric properties, the force transient was measured under constant strain. An example was shown in Fig. 4 (middle). The heating and cooling time constants were found by measuring the time taken for the force to reach 63.2% of the steady-state value during each step response. Fig. 8 shows the obtained time constants. It was found that both configurations showed moderate decrease in speed as size increased. 2D braided bundles were generally faster in the range of bundles tested, but the weaves appeared to slow down less significantly when scaled up.

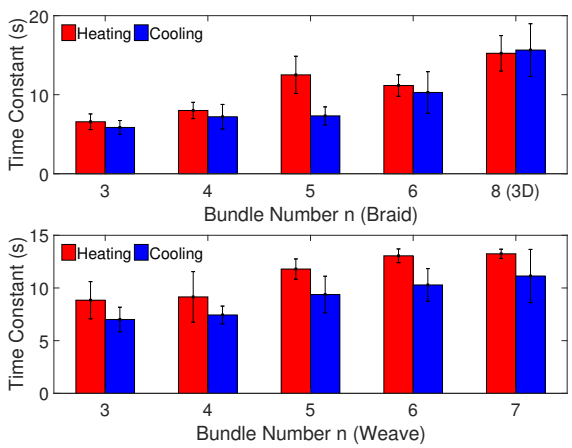

Fig. 8. Heating and cooling time constants of the bundled actuators with different configurations: Braided bundles (top) and woven bundles (bottom).

VI. Model Verification

To verify the accuracy of the model in Section V.E, the model was tested to estimate the strain of different bundled actuators under random power inputs consisting of multiple steps. An example of the steady-state power sequence was shown in Fig. 9 (top). Experimental measurements of the transient strain and corresponding steady state values were obtained, and compared to the strain from model estimation. As an example, Fig. 9 (middle) shows that the model could accurately estimate the strain outputs. Fig. 9 (bottom) shows the average verification error percentages against the number of actuators in each bundle. It was shown that the verification errors were consistently less than 13% for all sizes and configurations. Overall modeling verification errors were $10.99 \pm 8.28\%$ and $10.39 \pm 7.54\%$ for the braided and woven bundles, respectively. The verification errors were only slightly larger than the modeling error (Section VI.C), further validating the effectiveness of the proposed model.

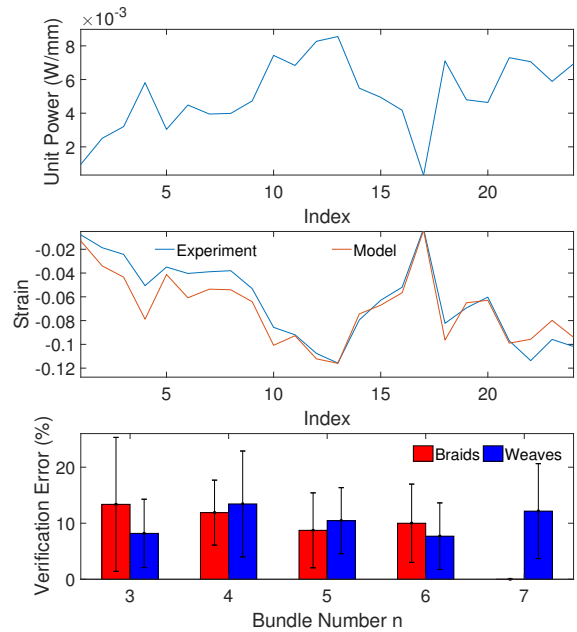

Fig. 9. A random input power sequence (top). Experimental and estimated strain for the 2D braided bundle with $n = 5$ (middle). Model verification error percentages (bottom).

VII. Discussion and Conclusion

In this work, three types of bundled SCP actuators have been designed and fabricated for force amplification. To learn their characteristics, we experimentally measured and compared the force, strain, and dynamical properties of the bundled actuators with different configurations. To further capture and estimate their performance metrics and study the scaling effects of the bundling methods, a model was proposed and experimentally validated. The results show that braids actuate faster and consume less power, weaves are geometrically appealing where a thin, flat profile is desired, and the stiff and powerful 3D braid may benefit high strength, low bandwidth applications.

The obtained numerical measurements, comparisons, and models can be utilized by other researchers and engineers who may wish to specify a particular bundled SCP actuator to apply in a robotic system. For instance, with a defined force and strain requirement, one can use a combination of Eq. (8) and Eq. (11)–(14) to compute the required power and bundle configuration combinations that enable their design. Eq. (4) and Eq. (5) can be used with certain desired bundle configurations to allow calculation in terms of the required power and range of motion. The specification can be further refined to incorporate dynamic range using Fig. 8. Defining a particular speed capability decreases the design space for which configurations and bundle sizes to consider when matching force and strain requirements using the relevant equations.

Future work can be conducted through more robust fabrication techniques, refined modeling, and design optimization of bundled actuators. First, thin polymer actuators like

SCP actuators show excellent promise for being mass manufactured and combined into textile-like configurations [10], [28]. With improved manufacturing, the accessibility of more refined design and fabrication will be possible. Second, with a simplified linear model, we acknowledge that the modeling errors shown in Fig. 6 and Fig. 9 are nontrivial. More in-depth nonlinear modeling will be studied to incorporate more bundle variables and capture the hysteresis. Thirdly, the task of more fully exploring how to tune the design parameters of each configuration for optimum performance will be studied together with more experiments considering different bundle configurations.

The following limitations of the study are summarized:

- While cotton string was used in the woven bundles, we acknowledge its thermally insulating nature could potentially hinder the weave performance. Thermally conductive weave materials could be considered.
- The slight inconsistencies of the actuators might have caused compromised performance. Since the fabrication was realized by hand, there were challenges for producing actuators with identical properties.
- Strain softening would be an effect study worth performing in the future to characterize how bundling behaviors vary over thousands to millions of cycles.
- Being thermally driven, SCP bundled actuators display low thermodynamic efficiency. Application of these actuators as robot muscles should carefully consider this property or use mechanisms such as a ratchet-and-locking structure to increase the efficiency.

References

[1] B. Tondu, "What is an artificial muscle? A systemic approach." *Actuators*, vol. 4, no. 4, pp. 336–352, 2015.

[2] P. E. Dupont, J. Lock, B. Itkowitz, and E. Butler, "Design and control of concentric-tube robots," *IEEE Trans. Robot.*, vol. 26, no. 2, pp. 209–225, 2010.

[3] Y. L. Park, B. R. Chen, N. O. Perez-Arancibia, D. Young, L. Stirling, R. J. Wood, E. C. Goldfield, and R. Nagpal, "Design and control of a bio-inspired soft wearable robotic device for ankle-foot rehabilitation," *Bioinspir. Biomim.*, vol. 9, no. 1, p. 016007, 2014.

[4] J. D. Greer, T. K. Morimoto, A. M. Okamura, and E. W. Hawkes, "Series pneumatic artificial muscles (sPAMs) and application to a soft continuum robot," in *Proc. IEEE/RSJ Int. Conf. Intell. Robot. Syst.*, 2017, pp. 5503–5510.

[5] J. Ueda, D. Ming, V. Krishnamoorthy, M. Shinohara, and T. Ogasawara, "Individual muscle control using an exoskeleton robot for muscle function testing," *IEEE Trans. Neural Syst. Rehabil. Eng.*, vol. 18, no. 4, pp. 339–350, 2010.

[6] J. D. Carrico, K. J. Kim, and K. K. Leang, "3D-printed ionic polymer-metal composite soft crawling robot," in *Proc. IEEE Int. Conf. Robot. Autom.*, 2017, pp. 4313–4320.

[7] M. D. Lima, N. Li, M. Jung de Andrade, S. Fang, J. Oh, G. M. Spinks, M. E. Kozlov, C. S. Haines, D. Suh, J. Foroughi, S. J. Kim, Y. Chen, T. Ware, M. K. Shin, L. D. Machado, A. F. Fonseca, J. D. W. Madden, W. E. Voit, D. S. Galvão, and R. H. Baughman, "Electrically, chemically, and photonically powered torsional and tensile actuation of hybrid carbon nanotube yarn muscles," *Science*, vol. 338, no. 6109, pp. 928–932, 2012.

[8] C. S. Haines, M. D. Lima, N. Li, G. M. Spinks, J. Foroughi, J. D. Madden, S. H. J. Kim, S. Fang, M. Jung de Andrade, F. Goktepe, O. Goktepe, S. M. Mirvakili, S. Naficy, X. Lepro, J. Oh, M. E. Kozlov, S. H. J. Kim, X. Xu, B. J. Swedlove, G. G. Wallace, and R. H. Baughman, "Artificial muscles from fishing line and sewing thread," *Science*, vol. 343, no. 6173, pp. 868–872, 2014.

[9] M. C. Yip and G. Niemeyer, "On the control and properties of supercoiled polymer artificial muscles," *IEEE Trans. Robot.*, vol. 33, no. 3, pp. 689–699, 2017.

[10] C. S. Haines, N. Li, G. M. Spinks, A. E. Aliev, J. Di, and R. H. Baughman, "New twist on artificial muscles," *Proc. Natl. Acad. Sci. USA*, vol. 113, no. 42, pp. 11 709–11 716, 2016.

[11] S. M. Mirvakili, A. Rafie Ravandi, I. W. Hunter, C. S. Haines, N. Li, J. Foroughi, S. Naficy, G. M. Spinks, R. H. Baughman, and J. D. W. Madden, "Simple and strong: twisted silver painted nylon artificial muscle actuated by joule heating," in *Proc. SPIE Electroactive Polymer Actuators and Devices*, vol. 9056, 2014.

[12] A. Abbas and J. Zhao, "A physics based model for twisted and coiled actuator," in *Proc. IEEE Int. Conf. Robot. Autom.*, 2017, pp. 6121–6126.

[13] J. Zhang, K. Iyer, A. Simeonov, and M. C. Yip, "Modeling and inverse compensation of hysteresis in supercoiled polymer artificial muscles," *IEEE Robot. Autom. Lett.*, vol. 2, no. 2, pp. 773–780, 2017.

[14] K. H. Cho, M. G. Song, H. Jung, J. Park, H. Moon, J. C. Koo, J. D. Nam, and H. R. Choi, "A robotic finger driven by twisted and coiled polymer actuator," in *Proc. SPIE Electroactive Polymer Actuators and Devices*, vol. 9798, 2016.

[15] L. Wu, M. J. de Andrade, L. K. Saharan, R. S. Rome, R. H. Baughman, and Y. Tadesse, "Compact and low-cost humanoid hand powered by nylon artificial muscles," *Bioinspir. Biomim.*, vol. 12, no. 2, p. 026004, 2017.

[16] Y. Almubarak and Y. Tadesse, "Twisted and coiled polymer (TCP) muscles embedded in silicone elastomer for use in soft robot," *Int. J. Intell. Robot. Appl.*, 2017.

[17] L. Sutton, H. Moein, A. Rafiee, J. D. W. Madden, and C. Menon, "Design of an assistive wrist orthosis using conductive nylon actuators," in *Proc. of IEEE Inter. Conf. Biomed. Robot. Biomech.*, 2016, pp. 1074–1079.

[18] M. Hiraoka, K. Nakamura, H. Arase, K. Asai, Y. Kaneko, S. W. John, K. Tagashira, and A. Omote, "Power-efficient low-temperature woven coiled fibre actuator for wearable applications," *Sci. Rep.*, vol. 6, 2016.

[19] T. Kawamura, K. Takanaka, T. Nakamura, and H. Osumi, "Development of an orthosis for walking assistance using pneumatic artificial muscle: A quantitative assessment of the effect of assistance," in *Proc. IEEE Int. Conf. Rehab. Robot.*, 2013, pp. 1–6.

[20] J. M. Jani, M. Leary, A. Subic, and M. A. Gibson, "A review of shape memory alloy research, applications and opportunities," *Mater. Des.*, vol. 56, pp. 1078–1113, 2014.

[21] S. Kurumaya, H. Nabae, G. Endo, and K. Suzumori, "Design of thin McKibben muscle and multifilament structure," *Sensor. Actuat. A Phys.*, vol. 261, pp. 66–74, 2017.

[22] M. Mosley and C. Mavroidis, "Experimental nonlinear dynamics of a shape memory alloy wire bundle actuator," *J. Dyn. Sys. Meas. Contr.*, vol. 123, no. 1, pp. 103–112, 2001.

[23] T. Doi, S. Wakimoto, K. Suzumori, and K. Mori, "Proposal of flexible robotic arm with thin mckibben actuators mimicking octopus arm structure," *Proc. IEEE/RSJ Int. Conf. Intell. Robot. Syst.*, pp. 5503–5508, 2016.

[24] T. E. Jenkins, E. M. Chapman, and M. Bryant, "Bio-inspired online variable recruitment control of fluidic artificial muscles," *Smart Mater. Struct.*, vol. 25, no. 12, p. 125016, 2016.

[25] S. A. DeLaHunt, T. E. Pillsbury, and N. M. Wereley, "Variable recruitment in bundles of miniature pneumatic artificial muscles," *Bioinspir. Biomim.*, vol. 11, no. 5, p. 056014, 2016.

[26] J. Abel, J. Luntz, and D. Brei, "A two-dimensional analytical model and experimental validation of garter stitch knitted shape memory alloy actuator architecture," *Smart Mater. Struct.*, vol. 21, no. 8, p. 085011, 2012.

[27] J. Foroughi, G. Spinks, S. Aziz, A. Mirabedini, A. Jeiranikhameneh, G. Wallace, M. Kozlov, and R. H. Baughman, "Knitted carbon-nanotube-sheath/spandex-core elastomeric yarns for artificial muscles and strain sensing," *ACS Nano*, vol. 10, no. 10, pp. 9129–9135, 2016.

[28] A. Maziz, A. Concas, A. Khaldi, J. Stålhand, N. K. Persson, and E. W. H. Jager, "Knitting and weaving artificial muscles," *Sci. Adv.*, vol. 3, no. 1, 2017.

[29] K. Sahashi, *Exquisite: the world of Japanese kumihimo braiding*. Kodansha International, 1988.

[30] J. Zhang, A. Simeonov, and M. C. Yip, "Three-dimensional hysteresis compensation enhances accuracy of robotic artificial muscles," *Smart Mater. Struct.*, [Online]. Available: http://iopscience.iop.org, DOI: 10.1088/1361-665X/aaa690.

[31] J. Weijde, B. Smit, M. Fritschi, C. Kamp, and H. Vallery, "Self-sensing of deflection, force, and temperature for joule-heated twisted and coiled polymer muscles via electrical impedance," *IEEE/ASME Trans. Mech.*, vol. 22, no. 3, pp. 1268–1275, 2017.